

Journal of Materials Chemistry A

Accepted Manuscript



This is an *Accepted Manuscript*, which has been through the Royal Society of Chemistry peer review process and has been accepted for publication.

Accepted Manuscripts are published online shortly after acceptance, before technical editing, formatting and proof reading. Using this free service, authors can make their results available to the community, in citable form, before we publish the edited article. We will replace this *Accepted Manuscript* with the edited and formatted *Advance Article* as soon as it is available.

You can find more information about *Accepted Manuscripts* in the [Information for Authors](#).

Please note that technical editing may introduce minor changes to the text and/or graphics, which may alter content. The journal's standard [Terms & Conditions](#) and the [Ethical guidelines](#) still apply. In no event shall the Royal Society of Chemistry be held responsible for any errors or omissions in this *Accepted Manuscript* or any consequences arising from the use of any information it contains.



A Template-free Synthesis for the Hierarchical Hydroxymethyl PEDOT Tube-Coral Array and Its Application in Dye-Sensitized Solar Cells

Yi-Feng Lin,^{‡a} Chun-Ting Li^{‡b} and Kuo-Chun Ho^{*ab}

Received 00th January 20xx,
Accepted 00th January 20xx

DOI: 10.1039/x0xx00000x

www.rsc.org/

A film of the hierarchical poly(hydroxymethyl 3,4-ethylenedioxythiophene) tube-coral array (PEDOT-MeOH TCA) was successfully synthesized via a template-free electro-polymerization technique. Via a four-stage growth mechanism, the PEDOT-MeOH TCA was designed to simultaneously possess (1) the enhanced conjugation on PEDOT main chain due to the electro-donating MeOH group, (2) the decreased energy band gap due to the elevated highest occupied molecular orbital level contributed by the electro-donating MeOH group, (3) the tube-like fast one-dimensional (1D) charge transfer pathways, and (4) the coral-like extended electro-active sites. For the application in dye-sensitized solar cells (DSSCs), PEDOT-MeOH TCA worked as an outstanding electro-catalytic counter electrode (CE) for iodine/triiodine (I/I_3^-) reduction. Thus, the DSSCs with the hierarchical PEDOT-MeOH TCA as the CE reached the highest solar-to-electricity conversion efficiency (η) of $9.13 \pm 0.06\%$, which was even higher than that of the DSSC with a standard Pt CE ($8.94 \pm 0.07\%$). Via various electro-chemical analyses (including cyclic voltammetry (CV), rotating disk electrode (RDE), four-point probe, Tafel polarization plots, and electrochemical impedance spectroscopy (EIS) techniques), the newly synthesized PEDOT-MeOH TCA film was found to have a lower intrinsic heterogeneous charge-transfer rate constant (k^0), extremely larger effective electro-catalytic surface area (A_e), and comparable sheet resistance (R_{sh}) than that of the standard Pt film. The PEDOT-MeOH TCA can be considered as a convincing replacement of the expensive Pt due to its high electro-catalytic ability, low cost, and simple fabrication process.

1. Introduction

In recent years, conducting polymers (CPs), including poly(3,4-ethylenedioxythiophene) (PEDOT),¹ poly(3,4-propylenedioxythiophene) (PProDOT),² polypyrrole,³ and polyaniline⁴ have become superior materials for various electrochemical devices, e.g., super-capacitors,⁵ lithium batteries,⁶ and solar cells.⁷ Among all the CPs, PEDOT is the most attractive CP due to its low-cost, environmental friendly property, high conductivity, good electrochemical reactivity, and good stability.⁸⁻¹⁰ However, the PEDOT-based films often have the flat or porous morphologies, which both lack of orientated or low-dimensional charge/electron transfer pathways; thus, the electrochemical performances of those PEDOT-based films are limited. Accordingly, structured PEDOT films were intensively designed and synthesized to have various morphologies such as nanorod,^{11, 12} nanotube (NT),¹³ and hollow microflower array

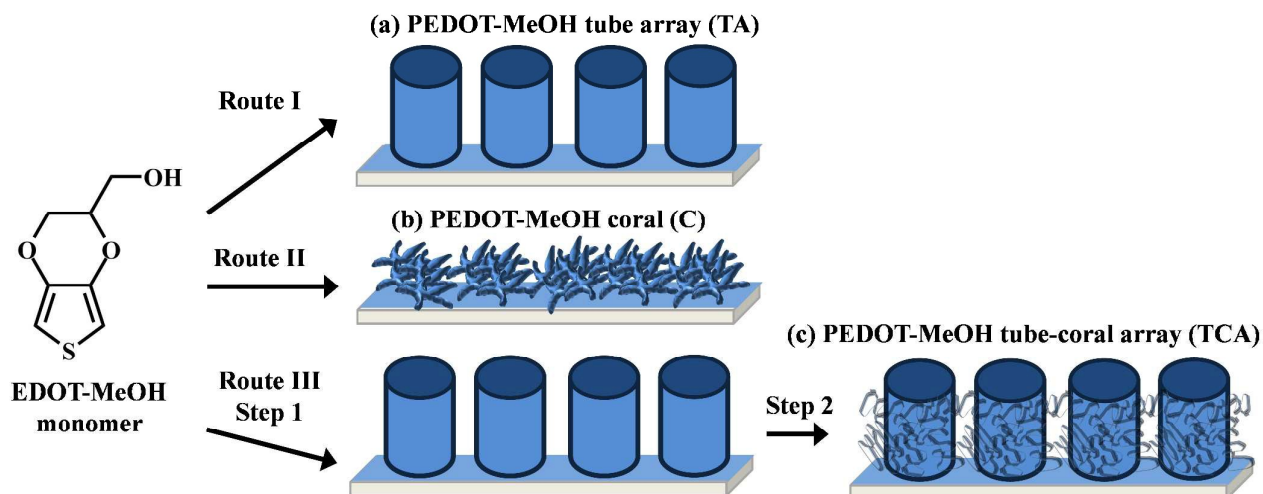
(HMFA)¹⁴ etc., via several synthetic routes using sacrificial templates (hard-templates or soft-templates).^{15, 16} It is noticed that the usages of the sacrificial templates bring two key disadvantages to the films: (1) a severe structural damage of the film during the removal of the sacrificial templates; (2) the inevitable and large decrease in the conductivity of the film due to the residual templates. In brief, in order to improve the electrochemical performances of the PEDOT-based films, a template-free synthesis for the structured PEDOT-based films is highly required.¹⁷

In this study, we establish a template-free and bottom-up electro-polymerization technique to obtain various structured PEDOT-based films using a hydromethyl functionalized EDOT monomer (EDOT-MeOH); the obtained films are generally denoted as PEDOT-MeOH. Via three routes, the PEDOT-MeOH tube array (TA), coral (C) and tube-coral array (TCA) films are separately synthesized as shown in **Scheme 1**. Furthermore, these three PEDOT-MeOH films were used as the counter electrodes (CEs) in dye-sensitized solar cells (DSSCs). In a DSSC, an effective CE aims to rapidly catalyze the triiodide (I_3^-) reduction.¹⁸ Since the traditional electro-catalyst, platinum (Pt), is very expensive and rare on earth, PEDOT-based materials have great potentials to replace Pt.¹⁹ As summarized in **Table 1**, chemically functionalized PEDOT²⁰⁻²⁵

^a Institute of Polymer Science and Engineering, National Taiwan University, No. 1, Sec. 4, Roosevelt Road, Taipei 10617, Taiwan. E-mail: kcho@ntu.edu.tw; Tel: +886-2-2366-0739; Fax: +886-2-2362-3040.

^b Department of Chemical Engineering, National Taiwan University, No. 1, Sec. 4, Roosevelt Road, Taipei 10617, Taiwan. E-mail: kcho@ntu.edu.tw; Tel: +886-2-2366-0739; Fax: +886-2-2362-3040.

Electronic supplementary information (ESI) available: More materials characterizations and electrochemical properties. See DOI: 10.1039/x0xx00000x
‡ These authors contributed equally.



Scheme 1 Synthetic routes of different PEDOT-MeOH films on FTO substrates. Route I was done under a constant voltage of 1.4 V (vs. Ag/Ag⁺) for 80 s at 0 °C in a DCM-based electrolyte containing 10.0 mM EDOT-MeOH monomer and 0.1 M TBAP. Route II was done under a constant voltage of 1.4 V (vs. Ag/Ag⁺) for 4 s at 25 °C in an ACN-based electrolyte containing 10.0 mM EDOT-MeOH monomer and 0.1 M LiClO₄. Route III contains two steps: step 1 corresponds to route I, while step 2 corresponds to route II.

Table 1 A partial literature review of the DSSCs' performance with PEDOT-based counter electrodes.

Electro-catalytic film on the counter electrode	η (%)	η (%) of Pt	Ref.
TsO ^a -doped PEDOT	4.60	4.67	[20]
ClO ₄ ^b -doped PEDOT	4.20	4.30	[21]
EMIB(CN) ₄ ^c -doped PEDOT	5.70	8.00	[22]
BMITFSI ^d -doped PEDOT	7.93	8.71	[23]
HMITFSI ^e -doped PEDOT	8.87	8.09	[24]
APS ^f -SiW ₁₁ ^g -codoped PEDOT	5.93	5.94	[25]
PEDOT-NT	8.30	8.50	[13]
PEDOT-HMFA	7.20	7.61	[14]
PEDOT-MeOH TCA	9.13	8.94	This work

^aTsO (Fe(III) tris-*p*-toluenesulfonate); ^bClO₄ (perchlorate); ^cEMIB(CN)₄ (1-ethyl-3-methylimidazolium tetracyano-borate); ^dBMITFSI (1-butyl-3-methyl-imidazolium bis(trifluoromethylsulfonyl)imide); ^eHMITFSI (hexyl-3-methylimidazolium bis(trifluoromethylsulfonyl) imide); ^fAPS (3-aminopropyltriethoxysilane); ^gSiW₁₁ (α -Keggin silicotungstates K₈[SiW₁₁O₃₉]·13H₂O).

films often gave good solar-to-electricity conversion efficiencies (η) to their cells because the functional groups benefit the conjugation of the PEDOT polymer main chains. The structured PEDOT (e.g., PEDOT-NT¹³ and PEDOT-HMFA¹⁴) films also achieve good η 's because they possess the fast and oriented charge transfer passages. However, it is hard to control structures of PEDOT without template. Since those structured PEDOT (NT and HMFA) were constructed via a template-assistant process (using ZnO as the template), their DSSCs only possess the comparable cell efficiencies with that of Pt.

In the case of our newly designed PEDOT-MeOH TCA, various advantages can be obtained simultaneously: (1) an enhanced conjugation of the PEDOT main chain due to the electro-donating MeOH group,^{26, 27} (2) the decreased energy band gap due to the elevated highest occupied molecular orbital (HOMO) level contributed by the electro-donating MeOH group,^{28, 29} (3) the fast one-dimensional charge transfer routes, (4) the extended electro-active sites. Finally, the PEDOT-MeOH TCA renders its DSSC a high η of 9.13 ± 0.06%, which is even higher than that of the Pt-based DSSC (8.94 ± 0.07%).

2. Experimental details

2.1 Materials

Hydroxymethyl 3,4-ethylenedioxythiophene (EDOT-MeOH, 95%), tetrabutylammonium perchlorate (TBAP, ≥ 99.0%), titanium (IV) tetraisopropoxide (TTIP, > 98%), ethanol (EtOH, 99.5%), isopropyl alcohol (IPA, 99.5%), lithium perchlorate (LiClO₄, ≥ 98.0%), tetrabutylammonium triiodide (≥ 97.0%), 2-methoxyethanol (≥ 99.5%), 3,4-ethylenedioxythiophene (EDOT, 97%), and tetramethylammonium perchlorate (TMAP, ≥ 99.0%) were obtained from Sigma Aldrich. Lithium iodide (LiI, synthetic grade), iodine (I₂, synthetic grade), and poly(ethylene glycol) (PEG, MW~20,000) were purchased from Merck. Acetone (99%), guanidinium thiocyanate (GuSCN, ≥ 99%), 4-tert-butylpyridine (tBP, 96%), and tert-butyl alcohol (tBA, 96%) were bought from Acros. 3-Methoxypropionitrile (MPN, 99%) was procured from Alfa Aesar. 1,2-Dimethyl-3-propylimidazolium iodide (DMPII) was procured from Tokyo Chemical Industry Co., Ltd. Transparent TiO₂ paste (TL paste, Ti-nanoxide HT/SP, 13 nm), Surlyn[®] (SX1170-25, 25 μ m) and cis-diisothiocyanato-bis(2,2'-bipyridyl-4,4'-dicarboxylato) ruthenium (II) bis(tetrabutylammonium) (N719 dye)

were supplied by Solaronix (S.A., Aubonne, Switzerland). Acetonitrile (ACN, 99.99%) and dichloromethane (DCM, $\geq 99.8\%$) were received from J. T. Baker. The commercial light scattering TiO₂ particles, ST-41 with an averaged diameter of 200 nm, were obtained from Ishihara Sangyo, Ltd. Fluorine-doped tin oxide (FTO, TEC-7, 7 Ω sq.⁻¹) conducting glass was purchased from NSG America, Inc., New Jersey, USA.

2.2 Preparation of various films

FTO conducting glasses were first cleaned with a neutral cleaner and then washed with de-ionized water, acetone, and isopropanol sequentially. A standard Pt counter electrode was prepared by a direct current sputtering of Pt thin film on an FTO substrate for a thickness of 30 nm.²⁴ All PEDOT-MeOH films and all bare PEDOT films were electro-polymerized using a potentiostat/galvanostat (PGSTAT 30, Autolab, Eco-Chemie, the Netherlands) in a three-electrode electrochemical system. A cleaned FTO substrate (1 cm²), a Pt foil, and an Ag/Ag⁺ electrode were used as the working, counter, and reference electrodes, respectively. Via three different electro-polymerization routes, three kinds of PEDOT-MeOH films with various morphologies were obtained. As shown in **Scheme 1**, route I aims to synthesize a PEDOT-MeOH tube array (PEDOT-MeOH TA) perpendicularly grown on the FTO substrate; and route I was done under a constant voltage of 1.4 V (*vs.* Ag/Ag⁺) for 80 s at 0 °C in a DCM-based electrolyte containing 10.0 mM EDOT-MeOH monomer and 0.1 M TBAP. Route II was used to synthesize a porous PEDOT-MeOH coral (PEDOT-MeOH C) structure on the FTO under a constant voltage of 1.4 V (*vs.* Ag/Ag⁺) for 4 s at 25 °C in an ACN-based electrolyte containing 10.0 mM EDOT-MeOH monomer and 0.1 M LiClO₄. Route III combined route I and route II sequentially; thus the PEDOT-MeOH TA is covered by a porous layer of PEDOT-MeOH C to form a hierarchical PEDOT-MeOH tube-coral array (PEDOT-MeOH TCA). Finally, three kinds of PEDOT-MeOH films, including PEDOT-MeOH TA, PEDOT-MeOH C, and PEDOT-MeOH TCA were obtained. Via the same routes (routes I and II), two bare PEDOT films (using EDOT as the monomer in the electro-polymerization bathes) were separately prepared and denoted as PEDOT-I and PEDOT-II, respectively. Besides, another PEDOT-MeOH TA film (denoted as PEDOT-MeOH TA*) was prepared via route I using the tetramethylammonium perchlorate (TMAP) as a replacement of tetrabutylammonium perchlorate (TBAP) in the electro-polymerization bath. In other words, this PEDOT-MeOH TA* is prepared in a DCM-based electrolyte containing 10.0 mM EDOT-MeOH monomer and 0.1 M TMAP.

2.3 Characterizations of the films

Surface morphologies of the films were observed by field-emission scanning electron microscopy (FE-SEM, Nova NanoSEM 230, FEI, Oregon, USA) and transmission electron microscopy (TEM, JEM-1230, JEOL, Tokyo, Japan). Surface chemical analyses of the films were made by X-ray photoelectron spectroscopy (XPS, Thermo Scientific Theta

Probe, UK). The absorption spectra of a film were obtained by an ultraviolet-visible-near infrared spectrophotometer (UV-Vis-NIR, JASCO V-670, USA). Electro-catalytic abilities of the films for I₃⁻/I₂⁻ redox couple were estimated through cyclic voltammetry (CV) and rotating disk electrode (RDE) techniques. CV analysis was performed by the above-mentioned potentiostat/galvanostat using a three-electrode system in an ACN-based solution, containing 10.0 mM LiI, 1.0 mM I₂, and 0.1 M LiClO₄. Various electro-catalytic films were used as the working electrodes. A Pt foil and Ag/Ag⁺ electrode were used as the counter and reference electrode, respectively. The scan rate for CV analysis was set at 100 mV s⁻¹. RDE analysis was performed by a potentiostat (model 900B, CH Instruments) equipped with a modulated speed rotator (MSR, PINE Instrument Company) in ACN-based electrolyte containing 0.1 M LiClO₄ and 1.0 mM tetrabutylammonium triiodide. The glassy carbon electrode (GCE, Part #AFE7R9GCGC, PINE Instrument Company) coated with an electro-catalytic material was separately used as the working electrode, and a Pt wire and Ag/Ag⁺ electrode were used as the counter and reference electrode, respectively. The rotating speeds were controlled at 50, 100, 200, 400, 600, 800, and 1000 rpm. The scan rate for RDE analysis was set at 2 mV s⁻¹. The sheet resistances (*R*_{sh}), relating the electrical conductivities of the films, were measured by a four-point probe technique and were recorded by a Keithley's instrument (Keithley 2400, Keithley Instruments Inc., USA). Electrochemical properties of various electro-catalytic films could be quantified by using their symmetric cells through Tafel polarization plots (Tafel plots) and electrochemical impedance spectroscopy (EIS) analyses, which were obtained by a potentiostat/galvanostat (PGSTAT 30, Autolab, Eco-Chemie, the Netherlands). The scan rate for Tafel analysis was set at 50 mV s⁻¹. The impedance spectra was obtained using a FRA2 module between 10 mHz to 65 kHz with an AC amplitude of ± 10 mV. The electrolyte for Tafel and EIS analyses contains 1.2 M DMPII, 0.035 M I₂, 0.1 M GuSCN, and 0.5 M tBP in MPN/ACN (volume ratio of 1:4).

2.4 Fabrication and characterization of the DSSCs

Firstly, the TiO₂ colloid was prepared by adding 0.5 M aqueous TTIP to 0.1 M nitric acid aqueous solution with simultaneously stirring at 88 °C for 8 h, and then by heating to 240 °C for 12 h in an autoclave (PARR 4540, USA). The autoclaved solution was concentrated to contain 8 wt% crystalline TiO₂ nanoparticles (NPs) (*ca.* 20 nm) in the TiO₂ slurry. A TiO₂ paste for the light transparent layer (TL paste) was formed by adding 25 wt% PEG (with respect to TiO₂ NPs) to the previous TiO₂ slurry, while another TiO₂ paste for the light scattering layer (SL paste) was formed by adding 25 wt% PEG and 100 wt% ST-41 (with respect to TiO₂ NPs) to the previous TiO₂ slurry. The PEG was used for preventing the SL paste from being cracked during its casting on an FTO glass and also to control the pore size of the pertinent TiO₂ film.

Secondly, a cleaned FTO conducting surface was treated by spin coating 100 nm TiO₂ compact layer using a solution of TTIP in 2-methoxyethanol (weight ratio of 1:3). A 0.20 cm²

TiO₂ film, containing 10 μm of TL and 4 μm of SL, was coated on the treated FTO glass by a doctor blade technique using the above-mentioned TL and SL pastes, respectively; and each layer was separately sintered at 500 °C for 30 min in an ambient atmosphere.² After the sintering process, the TiO₂ film was immersed in a 5.0×10⁻⁴ M N719 dye solution (mixed solvent of ACN/tBA with a volume ratio of 1:1) at room temperature for 24 h. The TiO₂ photoanodes were coupled with various films as the counter electrodes; the photoanodes were separated from the counter electrodes by using a 25 μm-thick Surlyn[®] film as the spacer. The electrolyte, which contained 1.2 M DMPII, 0.035 M I₂, 0.1 M GuSCN, and 0.5 M tBP in MPN/ACN (volume ratio of 1:4), was injected into the gap between these two electrodes by capillarity.

Photovoltaic parameters of the DSSCs with various films as the counter electrodes were obtained by a potentiostat/galvanostat under 100 mW cm⁻². The DSSCs were illuminated by a class A quality solar simulator (XES-301S, AM1.5G, San-Ei Electric Co., Ltd., Osaka, Japan) and the incident light intensity (100 mW cm⁻²) was calibrated with a standard Si cell (PECSI01, Peccell Technologies, Inc.). The incident photon-to-current conversion efficiency (IPCE) curves of the DSSCs were obtained by the potentiostat/galvanostat and by another class A quality solar simulator (PEC-L11, AM1.5G, Peccell Technologies, Inc., Kanagawa, Japan) equipped with a monochromator (model 74100, Oriel Instrument, California, USA). The IPCE spectra were obtained under a monochromatic light illumination in the wavelength region of 400 to 800 nm; the incident radiation flux (ϕ) was obtained by using an optical detector (model 818-SL, Newport, California, USA) and a power meter (model 1916-R, Newport, California, USA).

3. Results and discussion

3.1 Morphology

Surface morphologies of various films were observed by FE-SEM and TEM images, as shown in Fig. 1 and Fig. 2. Fig. 1a shows an ultra-thin Pt film covered on the FTO surface, indicating the structure of the Pt film is mainly determined by the granular morphology of the FTO. As compared to other films, Pt film is the flattest one, suggesting an inferior electrochemical surface. Fig. 1b and Fig. 2a reveal a sub-micro-sized PEDOT-MeOH tube array (PEDOT-MeOH TA) vertically grown on a relatively compact thin layer of PEDOT-MeOH on the FTO. The tubes on the PEDOT-MeOH TA film possess a smooth surface with an average length of 5 μm and an average diameter of 700 nm. Since Fig. 2a clearly shows that PEDOT-MeOH TA is vertically grown on the FTO, it can be said that the one-dimensional (1D) electron transfer pathways are successfully built on the PEDOT-MeOH TA films. Besides, the FE-SEM images of the PEDOT-MeOH TA film prepared in the presence of tetramethylammonium perchlorate (TMAP), denoted as PEDOT-MeOH TA*, are shown in Fig. S1 in the Electronic Supplementary Information. The PEDOT-MeOH TA* film also possesses the vertically aligned tube arrays, which have tube length and diameter similar to those of the PEDOT-MeOH TA film (with TBAP). Thus, it is found that no

obvious changes can be observed by varying the alkyl chain length of the tetraalkylammonium cations.

Fig. 1c shows a highly porous and coral-like PEDOT-MeOH matrix (denoted as PEDOT-MeOH C); suggesting its sufficient electrochemical active areas. Fig. 1d reveals that the porous PEDOT-MeOH C is uniformly decorated on the PEDOT-MeOH TA; thus a hierarchical structure of PEDOT-MeOH tube-coral array (PEDOT-MeOH TCA) is observed.

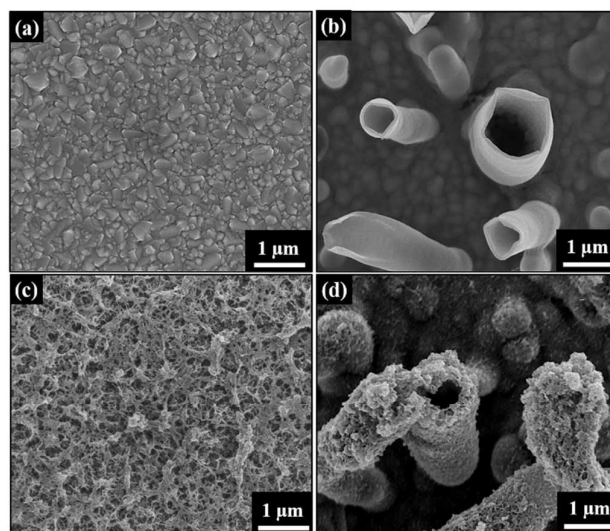


Fig. 1 Top-view FE-SEM images of the films of (a) Pt, (b) PEDOT-MeOH TA, (c) PEDOT-MeOH C, and (d) PEDOT-MeOH TCA.

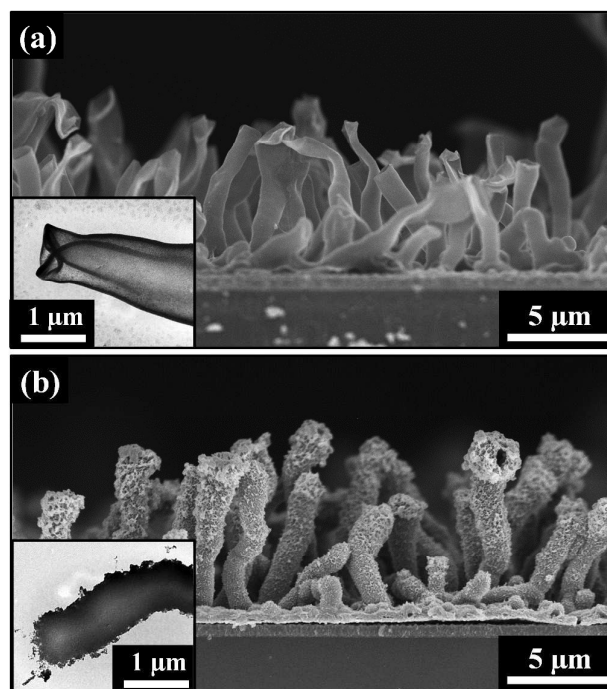


Fig. 2 Cross-sectional FE-SEM images of the films of (a) PEDOT-MeOH TA, and (b) PEDOT-MeOH TCA; their TEM images are shown in the insets correspondingly.

In the films of PEDOT-MeOH TCA, the inner PEDOT-MeOH TA layer provides 1D core to facilitate the electron transfer of the film, while the outer PEDOT-MeOH coral layer supplies extended active areas to multiply the electrochemical reaction flux. The tube-corals on the PEDOT-MeOH TCA film possess a highly porous surface with an average length of $5\ \mu\text{m}$ and an average diameter of 500 nm. Besides, **Fig. 2a** and **Fig. 2b** show the cross-sectional FE-SEM images of PEDOT-MeOH TA and PEDOT-MeOH TCA films, respectively; and their TEM images are shown in the insets correspondingly. Two key points can be once again verified by **Fig. 2**: (1) both of PEDOT-MeOH TA and PEDOT-MeOH TCA are indeed hollow tubular structure (see the insets); and (2) both of PEDOT-MeOH TA and PEDOT-MeOH TCA are vertically grown on their FTO substrates. In brief, via three simple and template-free routes, the PEDOT-MeOH films with various morphologies are successfully obtained. Especially for the newly designed PEDOT-MeOH TCA, it simultaneously possesses 1D electron transfer pathways and large active surfaces, suggesting its possible applications in various electrochemical electronics.

When it comes to the bare PEDOT films, the FE-SEM images of the PEDOT films prepared via route I (denoted as PEDOT-I, see **Fig. S2a** in the **Electronic Supplementary Information**) and route II (denoted as PEDOT-II, see **Fig. S2b**) show similar porous and coral-like morphology, which is the same as that of PEDOT-MeOH C. It is confirmed that the bare PEDOT films (without the hydroxymethyl functional groups) are not easy to have an orientated or 1D morphology.¹⁷ Therefore, the hydroxymethyl functional groups on the PEDOT-MeOH conducting polymer is very important to obtain the vertically aligned tube arrays on the films of PEDOT-MeOH TA and PEDOT-MeOH TCA.

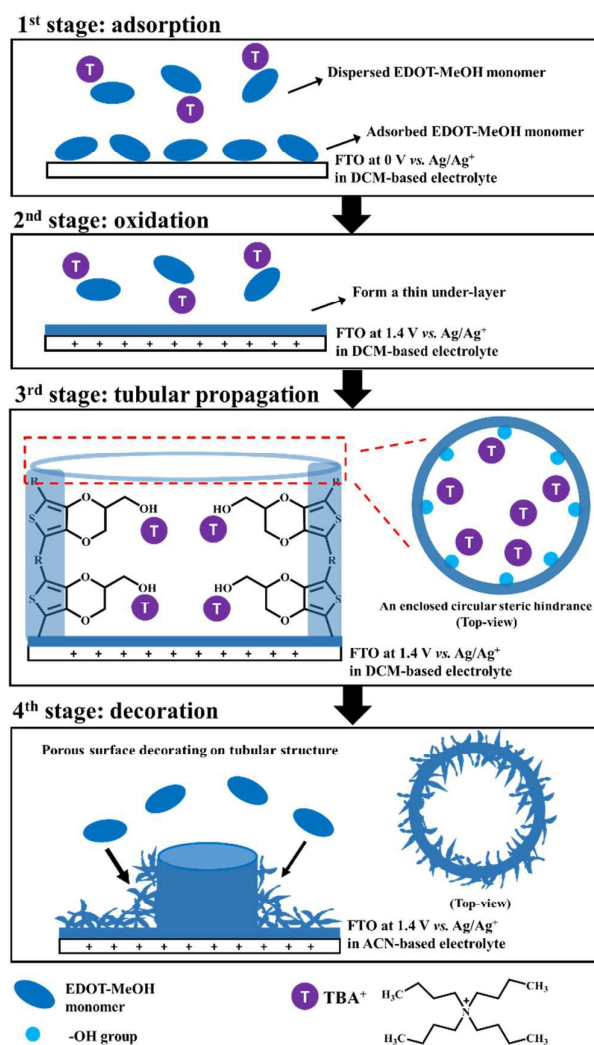
3.2 The effect of hydroxymethyl group on PEDOT-MeOH

To clarify the effect of the hydroxymethyl group on PEDOT-MeOH, we chose thin films of PEDOT-II and PEDOT-MeOH C for comparison since the preparation procedure and the morphology for these two films are the same. In other words, only the hydroxymethyl groups on the PEDOT-MeOH C can cause the difference for PEDOT-II and PEDOT-MeOH C films. From the absorption spectra (see **Fig. S2c**) of PEDOT-II and PEDOT-MeOH C films, both films give two distinct absorption bands in the visible (300~600 nm) and NIR (600~1300 nm) regions. The former corresponds to $\pi-\pi^*$ transition of a conducting polymer, while the latter is the transition between valence band and bipolaron band of a conducting polymer, which is related to its conjugation length.^{26, 27, 30} For a PEDOT-based film (PEDOT-II or PEDOT-MeOH C), the wavelengths (λ_1 and λ_2) of the maximum absorption peaks in the visible and NIR regions, respectively, are listed in the inset of **Fig. S2c**. It can be found that the values of λ_1 for both PEDOT-II and PEDOT-MeOH C films are very close, indicating the similar $\pi-\pi^*$ transition for both films. However, the values of λ_2 for PEDOT-MeOH C film (1229 nm) is larger than that for PEDOT-II film (894 nm), suggesting the obvious red-shift of the NIR absorption peak is caused by the hydroxymethyl

groups on the PEDOT-MeOH C film. This red-shift of the NIR absorption peak directly reflects the easier electron transition between valence band and bipolaron band of a conducting polymer; in other words, it reveals that the MeOH group can lead to both enhanced conjugation and the decreased energy band gap of a conducting polymer.²⁶⁻³⁰ Therefore, it is confirmed that PEDOT-MeOH C possesses longer conjugation length and better conjugation than those of PEDOT-II due to the existence of the hydroxymethyl groups on its polymer chain.

3.3 Growth mechanism of PEDOT-MeOH TCA film

Scheme 2 illustrates the four-stage growth mechanism of our newly synthesized PEDOT-MeOH TCA. In the 1st stage (without any applied voltage in the electro-polymerization cell), parts of the EDOT-MeOH monomers are statically adsorbed on the FTO surface, while other monomers are uniformly dispersed in a DCM-based electrolyte used in Route I (**Scheme 1**).



Scheme 2 The four-stage growth mechanism of PEDOT-MeOH TCA.

In the DCM-based electrolyte, a supporting electrolyte, tetrabutylammonium perchlorate (TBAP), is included. TBAP would dissociate into tetrabutylammonium cation (TBA^+) and perchlorate anion (ClO_4^-). TBA^+ would be attracted by the lone-pair electrons of the oxygen atoms on the EDOT-MeOH monomers. This can be simply denoted as the stage of “adsorption.” In the 2nd stage (with an applied voltage of +1.4 V vs. Ag/Ag^+ in the electro-polymerization cell), the adsorbed EDOT-MeOH monomers are quickly oxidized to form a thin under-layer of PEDOT-MeOH on the FTO, while the other monomers are moving toward the FTO substrate due to the driven electrical force. This can be simply denoted as the stage of “oxidation.” In the 3rd stage (with a continued applied voltage of +1.4 V vs. Ag/Ag^+ in the electro-polymerization cell), the monomers near the FTO are polymerized onto the under-layer; the pertinent PEDOT-MeOH chains are propagated along the normal direction of FTO due to the applied electrical field. During the electro-polymerization, some TBA^+ are simultaneously bonded to the oxygen atoms on the PEDOT-MeOH,³¹ which can be verified by N-O bond (at 401.55 eV) between the TBA^+ and PEDOT-MeOH polymer chain shown in the XPS spectrum (Fig. 3). Since the bonded TBA^+ and the hydroxyl groups on the PEDOT-MeOH are all hydrophilic, they tend to form an enclosed circular space, which works as a steric hindrance for the propagation of PEDOT-MeOH. When the applied voltage (+1.4 V vs. Ag/Ag^+) is continued, the PEDOT-MeOH tube array is thereby formed. This stage can be simply denoted as the stage of “tubular propagation.” In the 4th stage (in an ACN-based electrolyte used in Route II), the highly porous and coral-like PEDOT-MeOH matrix are irregularly decorated on the PEDOT-MeOH tube array due to the absence of the steric hindrance. This stage can be simply denoted as the stage of “decoration.” In summary, this four-stage growth mechanism of the PEDOT-MeOH TCA is proceeded in a sequence of adsorption \rightarrow oxidation \rightarrow tubular propagation \rightarrow decoration, as shown in Scheme 2.

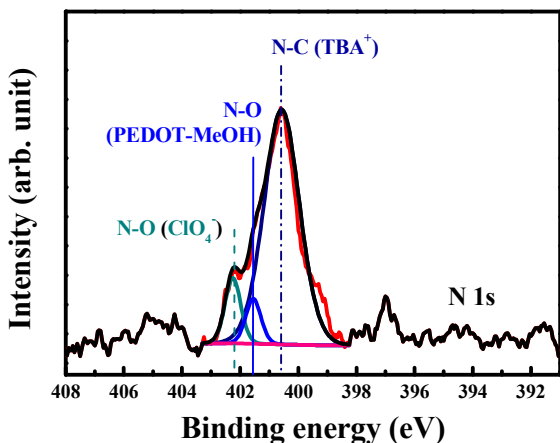


Fig. 3 XPS analysis of PEDOT-MeOH TCA film.

3.4 Photovoltaic performance of the DSSCs with various films as the CEs

For the application of the DSSCs, all synthesized PEDOT-MeOH films and a standard Pt film were used as the counter electrodes (CEs). In a DSSC, an electro-catalytic film on a CE aims to facilitate the heterogeneous charge transfer rate of Γ/I_3^- at the CE/electrolyte interface. A slow consumption of I_3^- can lead to the severe energy loss in a DSSC owing to the slow Γ regeneration, which cause the slow dye regeneration and the possible recombination reaction for the remaining I_3^- ions and the photo-induced electrons at the electrolyte/photoanode interface. Therefore, an effective electro-catalytic material as a CE to rapidly trigger the reduction of I_3^- becomes the key to obtain a highly efficient DSSC.³² An effective electro-catalytic material requires excellent electro-catalytic ability, good charge transfer capability, good conductivity, high corrosion resistivity, and good electrochemical stability.

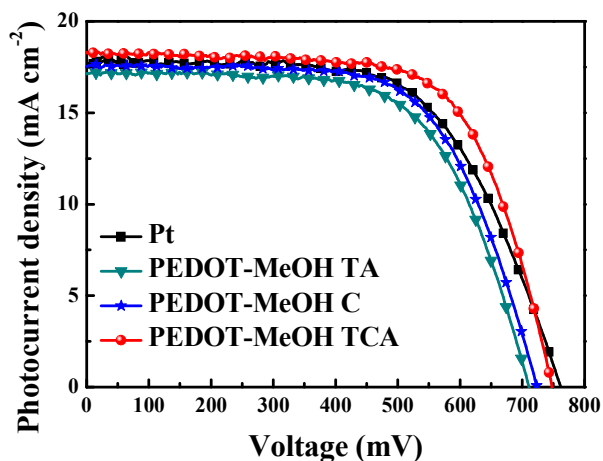


Fig. 4 Photocurrent density-voltage curves of DSSCs with various CEs measured at 100 mW cm^{-2} (AM 1.5G).

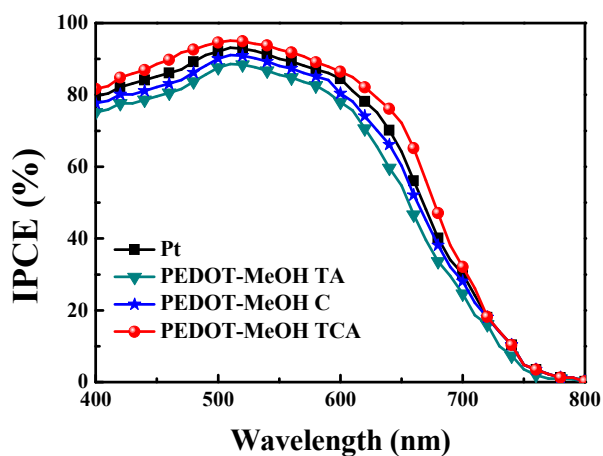


Fig. 5 IPCE curves of the DSSCs with various CEs.

Table 2 Photovoltaic parameters of the DSSCs with various CEs, measured at 100 mW cm⁻² (AM 1.5G). The standard deviation for each data is based on three DSSCs.

Electro-catalytic film on the counter electrode	η (%)	V_{OC} (mV)	J_{SC} (mA cm ⁻²)	FF	$J_{SC-IPCE}$ (mA cm ⁻²)
Pt	8.94 ± 0.07	748.00 ± 4.58	17.81 ± 0.14	0.67 ± 0.00	15.28
PEDOT-MeOH TA	7.85 ± 0.04	709.28 ± 1.41	17.22 ± 0.08	0.64 ± 0.00	14.00
PEDOT-MeOH C	8.23 ± 0.06	723.11 ± 2.44	17.57 ± 0.07	0.65 ± 0.00	14.74
PEDOT-MeOH TCA	9.13 ± 0.06	746.36 ± 1.41	18.22 ± 0.12	0.67 ± 0.00	16.02

Generally, platinum (Pt) works as the best electro-catalyst due to its outstanding electro-catalytic ability toward I₃⁻ reduction, so that Pt is the most frequently used and served as a standard CE in the DSSCs.³³

In **Fig. 4**, photocurrent density-voltage (J - V) curves of the DSSCs with various films (*i.e.*, standard Pt, PEDOT-MeOH TA, PEDOT-MeOH C, and PEDOT-MeOH TCA) as the CEs were measured at 100 mW cm⁻² illumination; the corresponding parameters are listed in **Table 2**. The DSSC coupled with the standard Pt as a CE shows an η of 8.94 ± 0.07% with an open-circuit voltage (V_{OC}) of 748.00 ± 4.58 mV, short-circuit current density (J_{SC}) of 17.81 ± 0.14 mA cm⁻², and fill factor (FF) of 0.67 ± 0.00. All cells with PEDOT-MeOH films as the CEs show good η 's of 7~9%, indicating a promising nature of this newly introduced PEDOT-MeOH material as the electro-catalyst toward I₃⁻ reduction. The PEDOT-MeOH TA CE gave its cell limited values of J_{SC} (17.22 ± 0.08 mA cm⁻²) and FF (0.64 ± 0.00) due to its smooth surface on the tubes (**Fig. 1b**) providing less active sites, while PEDOT-MeOH C CE also gave its cell limited J_{SC} (17.57 ± 0.07 mA cm⁻²) and FF (0.65 ± 0.00) due to its lack of 1D charge transfer pathways. When it comes to the hierarchical PEDOT-MeOH TCA CE, the co-existence of the 1D charge transfer pathways and large active surface areas on the PEDOT-MeOH TCA renders its DSSC the highest J_{SC} (18.22 ± 0.12 mA cm⁻²) and FF (0.67 ± 0.00) values than those of the cells with CEs of PEDOT-MeOH TA and PEDOT-MeOH C. It is surprised to find that the cell with PEDOT-MeOH TCA CE show a higher η (9.13 ± 0.06%) than that of Pt-based DSSC (8.94 ± 0.07%). The newly synthesized PEDOT-MeOH TCA film can be considered as a low-cost and convincing replacement of the expensive Pt.

In **Fig. 5**, the incident photon-to-current conversion efficiency (IPCE) spectra of the DSSCs with various films as the CEs are measured in a range of wavelength of 400-800 nm under the short-circuit condition. The maximum IPCE values of the cells with Pt, PEDOT-MeOH TA, PEDOT-MeOH C, and PEDOT-MeOH TCA are 93.1%, 88.6%, 91.1%, and 95.1% at 510 nm, respectively. It can be said that all PEDOT-MeOH and Pt films are efficient electro-catalytic materials to give their cells good performances. Moreover, an IPCE curve can be integrated to obtain a short-circuit current density ($J_{SC-IPCE}$), which is the summary of all the short-circuit current densities measured under individual monochromatic lights from 400 to 800 nm. In **Table 2**, the $J_{SC-IPCE}$ values for the DSSCs with Pt,

PEDOT-MeOH TA, PEDOT-MeOH C, and PEDOT-MeOH TCA CEs are 15.28, 14.00, 14.74, and 16.02 mA cm⁻², respectively. It can be concluded that the $J_{SC-IPCE}$ values obtained from IPCE curves (monochromatic spectrum) are in good agreement with the J_{SC} values obtained from the J - V curves (full sun-light spectrum).

3.5 Cyclic voltammetry and rotating disk electrode analyses of various films

To further precisely quantify the electro-catalytic ability of a CE, cyclic voltammetry (CV) and rotating disk electrode (RDE) analyses are separately performed in an I₃⁻/I₃⁻ redox electrolyte system. In the case of CV analysis, the major redox reactions at the electrolyte/CE interface include the oxidation of I⁻ (**Eqn. (1)**) and the reduction of I₃⁻ (**Eqn. (2)**)³⁴, which correspond to the anodic (J_{pa}) and cathodic (J_{pc}) peak current densities as shown in **Fig. 6**, respectively.



In **Fig. S3** in the **Electronic Supplementary Information**, the CVs curves of **Fig. 6** are shown individually; the corresponding background curves are included. Since a CE film is mainly used to trigger the reduction of I₃⁻ in a DSSC, the cathodic peak current density (J_{pc}), which is defined as the net current density at the peak, or the difference between the cathodic current peak and its background curve is focused. Higher value of J_{pc} directly reflects the better overall electro-catalytic ability of a film. In accordance with **Fig. S3**, the J_{pc} values of Pt, PEDOT-MeOH TA, PEDOT-MeOH C, and PEDOT-MeOH TCA films are 1.58, 1.13, 1.48, and 1.80 mA cm⁻², respectively, as summarized in **Table 3**. It can be observed that the film with higher J_{pc} gave the higher values of J_{SC} and FF to its DSSC (**Table 2**) due to the more charge transferring through the electrolyte/CE interface and the less charge recombination (energy loss) at the electrolyte/photoanode interface, respectively. Among all the films, PEDOT-MeOH TCA offers the highest J_{pc} value and thereby gives the highest J_{SC} , FF , and η to its DSSC, suggesting its better overall electro-catalytic ability than that of the standard Pt.

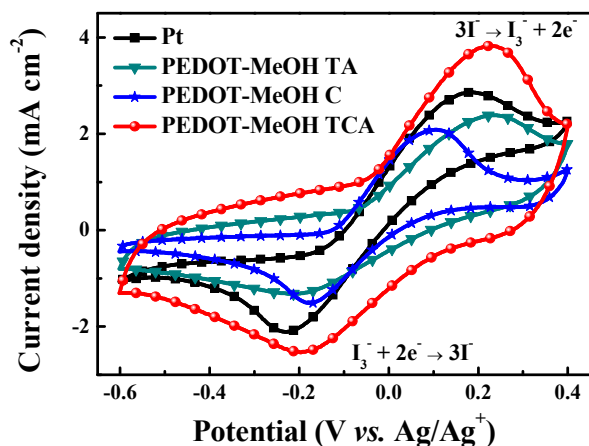


Fig. 6 Cyclic voltammograms of various films.

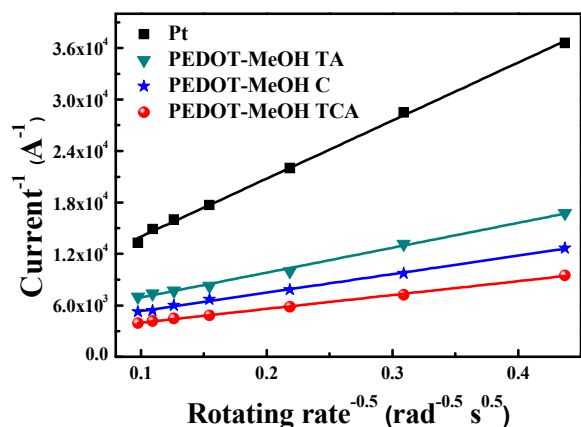


Fig. 7 Plots of i^{-1} vs. $\omega^{-0.5}$ of various films.

However, there are two key factors that influencing the overall electro-catalytic ability of a film, namely, the intrinsic heterogeneous charge-transfer rate constant (k^0) and the effective electro-catalytic surface area (A_e), which cannot be distinguished by the CV measurement. Here, the powerful RDE analysis aims to simultaneously quantify these two parameters. At seven rotating rates (50, 100, 200, 400, 600, 800, and 1000 rpm), a RDE coated with a given film was separately scanned to obtain seven pertinent linear sweep voltammetric (LSV) curves, which are used to give seven values of disk currents (i) at the formal potential (E^0) of Γ/I_3^- redox couple for a given film. The value E^0 of Γ/I_3^- redox couple at each film is determined by the above-mentioned CV curve (Fig. 6). When the rotating rates were converted into the angular velocity (ω), the plots of reciprocal disk current (i^{-1}) vs. reciprocal of rotating rate root ($\omega^{-0.5}$) were obtained for various films (i.e., Pt, PEDOT-MeOH TA, PEDOT-MeOH C, and PEDOT-MeOH TCA) as shown in Fig. 7. The intercept and slope of a fitting line in Fig. 7 were respectively used to find k^0 and A_e values by using the modified Koutecký–Levich equation shown in Eqn. (3)³⁵.

$$\frac{1}{i} = \frac{1}{nFA_e k^0 C} + \frac{1}{0.62nFA_e D^{2/3} \nu^{1/6} \omega^{1/2} C} \quad (3)$$

where i is the disk current obtained from the LSV curve at the formal potential (E^0), n is the number of electrons transferred, F is the Faraday constant, C is the concentration of I_3^- (1.0 mM), D is the diffusion coefficient of I_3^- ($3.62 \times 10^{-6} \text{ cm}^2 \text{ s}^{-1}$), ν is the kinematic viscosity of acetonitrile, and ω is the angular velocity converted from the rotating speed.

As summarized in Table 3, the standard Pt shows a k^0 value of $7.3 \times 10^{-3} \text{ cm s}^{-1}$, while all PEDOT-MeOH films show nearly the same k^0 value of $5.0 \times 10^{-3} \text{ cm s}^{-1}$, which is slightly lower than that of Pt (precisely, 0.70 times to that of Pt). On the other hand, the standard Pt gives the smallest A_e value of 0.19 cm^2 , while all PEDOT-MeOH films are able to provide larger A_e values, about 2–5.8 times to that of Pt owing to their rougher morphologies than that of Pt (Fig. 1). Among all the PEDOT-MeOH films, the values of A_e show a tendency of hierarchical PEDOT-MeOH TCA > PEDOT-MeOH C > PEDOT-MeOH TA, and thereby the J_{SC} and FF values of those DSSCs show the same trends. In brief, comparing Pt to all PEDOT-MeOH films, the Pt-based DSSCs show high performance due to the high k^0 of Pt. Among all PEDOT-MeOH films, the higher the values of J_{SC} and FF , the larger the values of A_e . Most importantly, hierarchical PEDOT-MeOH TCA provides good k^0 (0.70 times to Pt) and extremely large A_e (5.84 times to Pt) values, thus it gives better overall electro-catalytic ability than Pt. Although the thicknesses for all PEDOT-MeOH films are about two orders of magnitude thicker than that of the Pt film, the values of A_e provided by these PEDOT-MeOH films are 2–6 times higher than that of the Pt film. This phenomenon has been observed in many conducting polymers (with or without chemical dopants)^{36–38}, thus, it may be related to the intramolecular catalyzing mechanism of the conducting polymers, instead of the steric barriers for triiodide ions caused by the incorporation of tetrabutylammonium cations. In brief, the electro-catalytic abilities of the films shows the trend of PEDOT-MeOH TCA > Pt > PEDOT-MeOH C > PEDOT-MeOH TA, which is consistent with the trends obtained from both CV and RDE analyses.

3.6 Four-point probe measurements of various films

The sheet resistances (R_{sh}) of various films were obtained by the four-point probe method using the samples coated on the soda-lime glasses. The Pt film was directly sputtered on the soda-lime glass, while all PEDOT-MeOH films were gently removed from FTO glass by using H_2O_2 and the peeled films were put on the soda-lime glasses. Thus, the obtained R_{sh} values reflect only the resistivities of the films. The R_{sh} values for standard Pt, PEDOT-MeOH TA, PEDOT-MeOH C, and PEDOT-MeOH TCA are 6.18, 6.30, 7.34, and 6.21 $\Omega \text{ sq}^{-1}$, respectively (Table 3). It can be observed that the PEDOT-MeOH TA possesses a lower R_{sh} value than that of PEDOT-MeOH C, indicating that the PEDOT-MeOH TA has a larger electrical conductivity than that of PEDOT-MeOH C.

Table 3 Electrochemical parameters for various electro-catalytic films.

Electro-catalytic film on the counter electrode	J_{pc} (mA cm ⁻²)	k^0 (cm s ⁻¹)	A_e (cm ²)	R_{sh} (Ω sq. ⁻¹)	J_0 (mA cm ⁻²)	$R_{ct-Tafel}$ (Ω cm ²)	R_s (Ω cm ²)	R_{ct-EIS} (Ω cm ²)
Pt	1.58	7.3×10^{-3}	0.19	6.18	4.59	2.80	20.68	1.37
PEDOT-MeOH TA	1.13	5.0×10^{-3}	0.48	6.30	3.99	3.16	17.39	1.74
PEDOT-MeOH C	1.48	5.1×10^{-3}	0.65	7.34	4.39	2.92	19.35	1.44
PEDOT-MeOH TCA	1.80	5.1×10^{-3}	1.11	6.21	4.82	2.65	17.28	1.17

Accordingly, it is verified that the 1D sub-micro-sized tube array on PEDOT-MeOH-TA indeed works as the fast electron transfer passages. It can be found that the PEDOT-MeOH TA provides a faster electron transfer ability (~1.16 times than that of PEDOT-MeOH C) but a smaller electro-catalytic surface areas (~0.74 times than that of PEDOT-MeOH C); eventually, PEDOT-MeOH TA shows a lower overall electro-catalytic ability (lower J_{pc} obtained from CV) than that of PEDOT-MeOH C. As compared to the PEDOT-MeOH TA and PEDOT-MeOH C films, the hierarchical PEDOT-MeOH TCA film gives the lowest R_{sh} value due to the co-existence of the 1D tube array and the porous coral-like matrix.

3.7 Tafel polarization and electrochemical impedance spectra analyses of various films

To investigate the charge transfer properties at the electrolyte/CE interface in a practical DSSC, Tafel polarization and electrochemical impedance spectra (EIS) analyses were individually performed in the same electrolyte used for the photovoltaic measurement of the DSSCs. The electrolyte contains high Γ/I_3^- concentration (1.2 M DMPII, 0.035 M I_2 , 0.1 M GuSCN, and 0.5 M tBP in MPN/ACN with a volume ratio of 1:4). Here, a symmetrical cell, *i.e.*, a cell having the same film for both anode and cathode, is used for both Tafel and EIS analyses. In **Fig. 8**, Tafel polarization plots show the logarithmic current densities ($\log J$) as a function of voltage (V) for different films at a scan rate of 50 mV/s. In general, a Tafel curve is divided into three zones. The 1st part at low potentials ($|V| < 120$ mV, with a sharp slope) represents the polarization zone, the 2nd part at middle potentials (120 mV $< |V| < 400$ mV) represents the Tafel zone, and the 3rd part at high potentials ($|V| > 400$ mV, a horizontal part) represents the diffusion zone.³⁵ From **Fig. 8**, two charge transfer parameters can be obtained, namely, the exchange current density (J_0) and the charge transfer resistance ($R_{ct-Tafel}$). The value of J_0 of a film is read from the intercept (at $V=0$) of the extrapolating lines of both anodic and cathodic curves in Tafel zone. The J_0 value is tantamount to the electro-catalytic activity of a film; in other words, the higher J_0 represents the better electro-catalytic ability of a film. In **Table 3**, the values of J_0 show a tendency of hierarchical PEDOT-MeOH TCA $>$ Pt $>$ PEDOT-MeOH C $>$ PEDOT-MeOH TA, which is highly consistent with the values of J_{pc} obtained from CV measurement and is in good agreement

with the values of J_{SC} and FF obtained from the photovoltaic measurement.

Moreover, the J_0 value is further used to calculate the value of $R_{ct-Tafel}$ using **Eqn. (4)**.³⁵

$$J_0 = \frac{RT}{nFR_{ct-Tafel}} \quad (4)$$

where R is the ideal gas constant, T is the absolute temperature. The higher the value of J_0 , the smaller the value of $R_{ct-Tafel}$, indicating the more amount of electrons passing through the electrolyte/CE interface. In **Table 3**, the hierarchical PEDOT-MeOH TCA has the least $R_{ct-Tafel}$ value of 2.65 Ω cm², which is lower than that of PEDOT-MeOH TA (3.16 Ω cm²) and PEDOT-MeOH C (2.92 Ω cm²), because hierarchical PEDOT-MeOH TCA possesses both 1D electron transfer pathways and large active surfaces. Hierarchical PEDOT-MeOH TCA film even provides lesser $R_{ct-Tafel}$ value than that of Pt (2.80 Ω cm²), indicating its good charge transfer ability toward I_3^- reduction. Besides, all the J_0 and $R_{ct-Tafel}$ values were confirmed by their standard deviation values listed in **Table S1** in the **Electronic Supplementary Information**.

An electrochemical impedance spectrum (EIS) of a symmetric cell was performed based on an electro-catalytic film to extract three electrochemical parameters via fitting the spectrum into an equivalent circuit, as shown in the inset of **Fig. 9**. Firstly, the intercept of high-frequency semicircle with the horizontal axis represents the series resistance (R_s), which refers to the resistance across the electro-catalytic film/substrate interface. The R_s value is affected mainly by the conductivity of the electro-catalytic film and the adhesion between the film and its conducting substrate.³⁹ Secondly, the radius of high-frequency semicircle corresponds to the charge transfer resistance (R_{ct-EIS}) at the electro-catalytic film/electrolyte interface. Thirdly, the diameter of low-frequency semicircle (not obvious in **Fig. 9**) refers to the Warburg diffusion resistance (Z_w) within the bulk electrolyte. In **Fig. 9**, the low-frequency semicircle seems to be overlapped with the high-frequency semicircle; this is due to the short diffusion length for the redox species via using the thin cell spacer (25 μm-thick) and the low viscosity of the solvents for the electrolyte (the viscosities of ACN and MPN are 0.37 cp and 1.60 cp, respectively).³⁶

As summarized in **Table 3**, the R_s values for standard Pt, PEDOT-MeOH TA, PEDOT-MeOH C, and PEDOT-MeOH TCA are 20.68, 17.39, 19.35, and 17.28 $\Omega \text{ cm}^2$, respectively. All PEDOT-MeOH films (17.28–19.35 $\Omega \text{ cm}^2$) possess lower R_s values than that of Pt (20.68 $\Omega \text{ cm}^2$); this is mainly attributed to the better adhesion between a PEDOT-MeOH film and its substrate, compared to the adhesion between a Pt film and its substrate. It is believed that a better adhesion between a CE film and an FTO substrate is achieved using the electropolymerization synthesis (for all PEDOT-MeOH films), when comparing to that of the sputtered Pt film. The R_s values of PEDOT-MeOH TA and PEDOT-MeOH TCA are found to be similar and are both lower than that of PEDOT-MeOH C. Since all PEDOT-MeOH films are prepared by the electropolymerization process, the adhesions between these three films and their substrates are assumed to be the same. Thus, the lower R_s values of PEDOT-MeOH TA and PEDOT-MeOH TCA are expected to be attributed to their lower R_{sh} values (namely, better conductivities), as compared to those values of PEDOT-MeOH C.

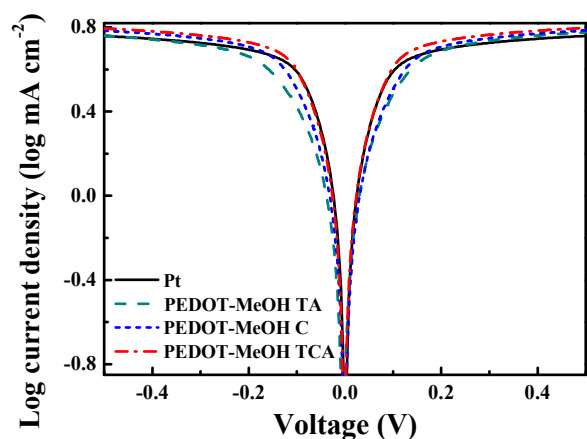


Fig. 8 Tafel polarization plots of various films.

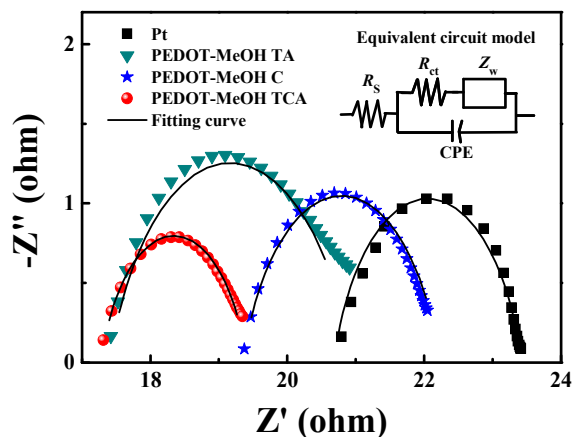


Fig. 9 Electrochemical impedance spectra of various films.

On the other hand, it is to be noted that all the R_{ct-EIS} values (obtained from EIS spectra) are consistent with the $R_{ct-Tafel}$ values (obtained from Tafel plots). And both R_{ct-EIS} and $R_{ct-Tafel}$ values, irrespective of their measurement techniques, show high consistency with the J_{pc} values obtained from CV and the J_0 values obtained from Tafel analysis; in other words, the electrocatalytic abilities of the films (PEDOT-MeOH TCA > Pt > PEDOT-MeOH C > PEDOT-MeOH TA) were precisely determined and consistently explained using CV, RDE, Tafel, and EIS analyses. Finally, the CE with hierarchical PEDOT-MeOH is believed to have a great potential to replace Pt.

Moreover, another EIS spectrum collected from a DSSC (FTO/photoanode/electrolyte/CE/FTO) is further used to support the results obtained from the EIS spectrum based on a symmetric cell. This type of EIS analysis is measured under one sun (*i.e.*, 100 mW cm^{-2} (AM1.5G)). Generally, an EIS spectrum performed on a DSSC contains three semicircles in accordance with the equivalent circuit shown in the inset of **Fig. S4** in the **Electronic Supplementary Information**. And four parameters can be extracted by fitting an EIS spectrum. (1) The intercept of high-frequency semicircle with the horizontal axis represents the series resistance (R_s^*), which includes (i) the conductivity of both photoanode and counter electrodes, (ii) the adhesion of a photoanode with its FTO substrate, and (iii) the adhesion of a CE with its substrate. (2) The diameter of the high-frequency semicircle represents the heterogeneous charge transfer resistance (R_{ct1}) at the CE/electrolyte interface. (3) The diameter of the middle-frequency semicircle refers to the heterogeneous charge transfer resistance (R_{ct2}) at the photoanode/electrolyte interface. (4) The diameter of the low-frequency semicircle corresponds to the Warburg diffusion coefficient (Z_w^*) between a photoanode and a CE.⁴⁰ In **Fig. S4**, the low-frequency semicircle for an EIS spectrum is also being overlapped, suggesting the negligible diffusion resistant within a cell. **Table S1** lists the values of R_s^* , R_{ct1} , and R_{ct2} . By using the same photoanode, the variation of R_s^* value is attributed to the differences in the conductivities of the CE films and the adhesions between the CE films and their substrates. The tendency of the R_s^* values obtained from the DSSCs containing various CE films shows great consistency with that of the R_s values obtained from the symmetric cells. In the case of R_{ct1} , the values of R_{ct1} for the DSSCs coupled with Pt, PEDOT-MeOH TA, PEDOT-MeOH C, and PEDOT-MeOH TCA CEs are 1.78, 2.46, 2.13 and 1.51 Ω , respectively; these R_{ct1} values give the similar trend with that of the R_{ct-EIS} values obtained from the EIS spectra based on the symmetric cells. In the case of R_{ct2} , the values of R_{ct2} for all the films are similar since the same photoanode is used.

For the best PEDOT-MeOH TCA film, it is clear that the PEDOT-MeOH TA film gives better conductivity (lower R_s^* and R_s), while the PEDOT-MeOH C film provides extremely larger effective surface area for the I_3^- reduction (larger A_e ; lower R_{ct1} and R_{ct-EIS}). In summary, the DSSC with PEDOT-MeOH TCA CE reached the highest J_{SC} , FF , and thereby the highest η due to the coexistence of the fast one-dimensional charge transfer routes and large extended electro-active sites.

4. Conclusions

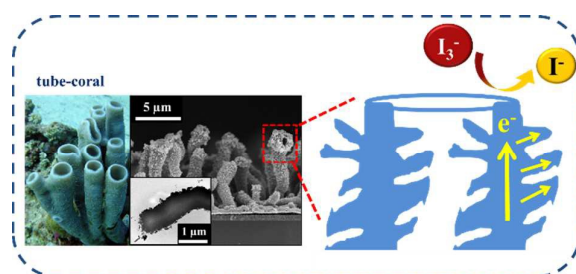
Films of poly(hydroxymethyl 3,4-ethylenedioxythiophene) (PEDOT-MeOH) with various morphologies were successfully synthesized by template-free preparations, and introduced for the first time as the counter electrodes in DSSCs. Among all the films, the highest electro-catalytic ability is given by the hierarchical PEDOT-MeOH tube-coral array (PEDOT-MeOH TCA) film owing to three key factors: (1) fast 1D charge transfer pathways provided by 1D tube-array structure, (2) extremely large active sites provided by porous surface, and (3) rapid reduction rate of I_3^- at the designed film. As regard to the key factor (1), the fast 1D electron transfer routes of the PEDOT-MeOH TCA film can be confirmed via its low sheet resistances (R_{sh}). As regard to the key factor (2), the large active sites of the PEDOT-MeOH TCA film can be proven via its large effective electro-catalytic surface area (A_e). As regard to the key factor (3), the rapid reduction rate of I_3^- at PEDOT-MeOH TCA film is verified by its large J_{pc} , large J_0 , low R_{ct} (both Tafel and EIS measurements), good k^0 , and extremely high A_e . Therefore, the DSSC with PEDOT-MeOH TCA exhibits the highest efficiency of $9.13 \pm 0.06\%$, which is even higher than that of the DSSC with a Pt film ($8.94 \pm 0.07\%$). It may be concluded that the PEDOT-MeOH TCA is a promising electro-catalytic material to replace the expensive Pt in DSSCs.

Acknowledgements

This work was supported by the Ministry of Science and Technology (MOST) of Taiwan, under grant numbers 102-2221-E-002-186-MY3 and 103-2119-M-007-012.

Notes and references

1. T. L. Zhang, H. Y. Chen, C. Y. Su and D. B. Kuang, *J. Mater. Chem. A*, 2013, **1**, 1724-1730.
2. K. M. Lee, P. Y. Chen, C. Y. Hsu, J. H. Huang, W. H. Ho, H. C. Chen and K. C. Ho, *J. Power Sources*, 2009, **188**, 313-318.
3. S. S. Jeon, C. Kim, J. Ko and S. S. Im, *J. Mater. Chem.*, 2011, **21**, 8146-8151.
4. W. W. Sun, T. Peng, Y. M. Liu, S. Xu, J. K. Yuan, S. S. Guo and X. Z. Zhao, *J. Mater. Chem. A*, 2013, **1**, 2762-2768.
5. Y. Zhou, N. Lachman, M. Ghaffari, H. P. Xu, D. Bhattacharya, P. Fattahi, M. R. Abidian, S. Wu, K. K. Gleason, B. L. Wardle and Q. M. Zhang, *J. Mater. Chem. A*, 2014, **2**, 9964-9969.
6. L. Yu, Z. Y. Wang, L. Zhang, H. B. Wu and X. W. Lou, *J. Mater. Chem. A*, 2013, **1**, 122-127.
7. H. M. Chuang, C. T. Li, M. H. Yeh, C. P. Lee, R. Vittal and K. C. Ho, *J. Mater. Chem. A*, 2014, **2**, 5816-5824.
8. S. Kirchmeyer and K. Reuter, *J. Mater. Chem.*, 2005, **15**, 2077-2088.
9. Q. B. Pei, G. Zuccarello, M. Ahlskog and O. Inganas, *Polymer*, 1994, **35**, 1347-1351.
10. A. A. Argun, A. Cirpan and J. R. Reynolds, *Adv. Mater.*, 2003, **15**, 1338-1341.
11. J. E. Lee, S. J. Park, O. S. Kwon, H. W. Shim, J. Jang and H. Yoon, *RSC Adv.*, 2014, **4**, 37529-37535.
12. H. A. Lin, S. C. Luo, B. Zhu, C. Chen, Y. Yamashita and H. H. Yu, *Adv. Funct. Mater.*, 2013, **23**, 3212-3219.
13. R. Trevisan, M. Dobbelin, P. P. Boix, E. M. Barea, R. Tena-Zaera, I. Mora-Sero and J. Bisquert, *Adv. Energy Mater.*, 2011, **1**, 781-784.
14. C. W. Kung, Y. H. Cheng, H. W. Chen, R. Vittal and K. C. Ho, *J. Mater. Chem. A*, 2013, **1**, 10693-10702.
15. Y. Z. Long, M. M. Li, C. Z. Gu, M. X. Wan, J. L. Duvail, Z. W. Liu and Z. Y. Fan, *Prog. Polym. Sci.*, 2011, **36**, 1415-1442.
16. Z. G. Yin and Q. D. Zheng, *Adv. Energy Mater.*, 2012, **2**, 179-218.
17. S. C. Luo, J. Sekine, B. Zhu, H. C. Zhao, A. Nakao and H. H. Yu, *ACS Nano*, 2012, **6**, 3018-3026.
18. B. Oregan and M. Grätzel, *Nature*, 1991, **353**, 737-740.
19. S. N. Yun, A. Hagfeldt and T. L. Ma, *Adv. Mater.*, 2014, **26**, 6210-6237.
20. Y. Saito, T. Kitamura, Y. Wada and S. Yanagida, *Chem. Lett.*, 2002, **10**, 1060-1061.
21. J. B. Xia, N. Masaki, K. J. Jiang and S. Yanagida, *J. Mater. Chem.*, 2007, **17**, 2845-2850.
22. J. M. Pringle, V. Armel and D. R. MacFarlane, *Chem. Commun.*, 2010, **46**, 5367-5369.
23. S. Ahmad, J. H. Yum, X. X. Zhang, M. Grätzel, H. J. Butt and M. K. Nazeeruddin, *J. Mater. Chem.*, 2010, **20**, 1654-1658.
24. C. T. Li, C. P. Lee, M. S. Fan, P. Y. Chen, R. Vittal and K. C. Ho, *Nano Energy*, 2014, **9**, 1-14.
25. C. C. Yuan, S. S. Guo, S. M. Wang, L. Liu, W. L. Chen and E. B. Wang, *Ind. Eng. Chem. Res.*, 2013, **52**, 6694-6703.
26. X. H. Zhang, S. S. Wang, S. Lu, J. Su and T. He, *J. Power Sources*, 2014, **246**, 491-498.
27. J. T. Lei, Z. H. Cai and C. R. Martin, *Synt. Met.*, 1992, **46**, 53-69.
28. X. M. Ma, W. Q. Zhou, D. Z. Mo, K. X. Zhang, Z. P. Wang, F. X. Jiang, D. F. Hu, L. Q. Dong and J. K. Xu, *J. Electroanal. Chem.*, 2015, **743**, 53-59.
29. L. P. Wu, L. M. Lu, L. Zhang, J. K. Xu, K. X. Zhang, Y. P. Wen, X. M. Duan and F. Yang, *Electroanalysis*, 2013, **25**, 2244-2250.
30. C. H. Chiang, S. C. Chen and C. G. Wu, *Org. Electron.*, 2013, **14**, 2369-2378.
31. F. S. Mjalli, J. Naser, B. Jibril, V. Alizadeh and Z. Gano, *J. Chem. Eng. Data*, 2014, **59**, 2242-2251.
32. S. Thomas, T. G. Deepak, G. S. Anjusree, T. A. Arun, S. V. Nair and A. S. Nair, *J. Mater. Chem. A*, 2014, **2**, 4474-4490.
33. K. Saranya, M. Rameez and A. Subramania, *Eur. Polym. J.*, 2015, **66**, 207-227.
34. M. X. Wu, X. Lin, Y. D. Wang, L. Wang, W. Guo, D. D. Qu, X. J. Peng, A. Hagfeldt, M. Grätzel and T. L. Ma, *J. Am. Chem. Soc.*, 2012, **134**, 3419-3428.
35. A. J. Bard and L. R. Faulkner, *Electrochemical Methods: Fundamentals and Applications*, John Wiley & Sons. Inc., 2nd edn., 2001.
36. L. Y. Chang, C. T. Li, Y. Y. Li, C. P. Lee, M. H. Yeh, K. C. Ho and J. J. Lin, *Electrochim. Acta*, 2015, **155**, 263-271.
37. K. M. Lee, C. Y. Hsu, P. Y. Chen, M. Ikegami, T. Miyasaka and K. C. Ho, *Phys. Chem. Chem. Phys.*, 2009, **11**, 3375-3379.
38. P. W. Chen, C. P. Lee, L. Y. Chang, J. Chang, M. H. Yeh, L. Y. Lin, R. Vittal, J. J. Lin and K. C. Ho, *RSC Adv.*, 2013, **3**, 5871-5881.
39. Q. Wang, S. Ito, M. Grätzel, F. Fabregat-Santiago, I. Mora-Sero, J. Bisquert, T. Bessho and H. Imai, *J. Phys. Chem. B*, 2006, **110**, 25210-25221.
40. F. Fabregat-Santiago, G. Garcia-Belmonte, I. Mora-Sero and J. Bisquert, *Phys. Chem. Chem. Phys.*, 2011, **13**, 9083-9118.

*Graphical Abstract***A Template-free Synthesis for the Hierarchical Hydroxymethyl PEDOT Tube-Coral Array and Its Application in Dye-Sensitized Solar Cells**Yi-Feng Lin^a, Chun-Ting Li^b, and Kuo-Chuan Ho^{a,b,*}^a *Institute of Polymer Science and Engineering, National Taiwan University, Taipei 10617, Taiwan*^b *Department of Chemical Engineering, National Taiwan University, Taipei 10617, Taiwan*

Hierarchical PEDOT-MeOH tube-coral array counter electrode (CE) rendered a good cell efficiency of 9.13% to its dye-sensitized solar cell, suggesting its potential to replace the traditional expensive Pt CE.